Detection of OH(X,v'',J'') via the $B\ ^2\Sigma^+ - X\ ^2\Pi$ Transition and Properties of the $B\ ^2\Sigma^+$ State

Eunsook S. Hwang and Jennifer B. Lipson

Stewart Radiance Laboratory, Bedford, Massachusetts 01730

Robert W. Field

Department of Chemistry, Massachusetts Institute of Technology, Cambridge, Massachusetts 02139

James A. Dodd*

*Air Force Research Laboratory, Space Vehicles Directorate,
Hanscom Air Force Base, Massachusetts 01731-3010*

A number of OH $B\ ^2\Sigma^+ - X\ ^2\Pi$ vibration−rotation spectra have been obtained using laser-induced fluorescence (LIF). Vibrationally excited OH($X,v'' = 6-9$) was formed through the reaction of H with O_3, and the v'',J''-dependent populations were characterized through synthetic spectral fitting of the $B-X$ $0-v''$ spectral data. The populations have been partially relaxed by collisions in the source region. The OH($B-X$) $0-v''$ relative band intensities have been determined and agree with previous theoretical values. Several OH($B,v' = 0$) J'-dependent collision-free lifetimes have been measured; the lifetimes decrease rapidly with J'. The $B\ ^2\Sigma^+$ state is weakly predissociated through a combination of spin−orbit and **L**-uncoupling ("gyroscopic") perturbation interactions with the nearby $2\ ^2\Pi$ state. Although the OH $B-X$ LIF technique cannot be used to monitor high rotational levels, it is well-suited for detecting the populations of high vibrational levels of the $X\ ^2\Pi$ state because of favorable Franck−Condon overlap. It also allows for operation at much lower reactant densities than is possible using the less sensitive OH chemiluminescence detection technique, mitigating the risk of unforeseen chemistry from metastable−metastable reactions. These results should add confidence in deriving accurate OH $X\ ^2\Pi$ v'',J''-dependent populations from $B-X$ spectra.

Introduction

The OH Meinel bands form an intense, spectrally highly structured nighttime emission source in the vicinity of the earth's mesopause, roughly centered at 87 km with a 5−7 km altitude spread. The emissions, due to fundamental and overtone transitions of vibrationally excited hydroxyl, are composed of hundreds of lines that extend from the red portion of the visible spectrum out to 5 μm in the mid-IR. The vibrationally excited OH is formed via the reaction

$$H + O_3 \rightarrow OH(X\ ^2\Pi, v'' \leq 9) + O_2 \qquad (1)$$
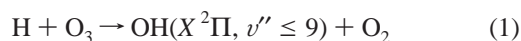
Predicting the radiance level and spectral distribution of the OH-(v'') emission relies on an accurate knowledge of such kinetic parameters as the reaction rate constant, the OH(v'') nascent product distribution, and the quenching rates and pathways for the nascently formed OH(v''). Measuring the nascent OH vibrational and rotational state distribution of reaction 1 has been the object of several experimental investigations since Polanyi and co-workers' landmark study.[1,2] The dynamics of the H + O$_3$ reaction, including the OH product state distribution, have also been examined using theory.[3,4]

All of the nascent product studies of reaction 1 have employed IR chemiluminescence detection, taking advantage of the strong OH($X\ ^2\Pi$) fundamental and overtone emissions. The chemiluminescence detection method is straightforward experimentally

and provides data that is easily interpreted in terms of the emitting populations in the various v'' and J'' states. However, it is many orders of magnitude less sensitive than laser-induced fluorescence (LIF) detection. Measurement of the quenching rates and especially the pathways, i.e., whether collisions induce single or multiquantum vibrational relaxation, is more easily accomplished using laser techniques to excite selectively and to detect individual vibration−rotation levels. The greater sensitivity of the LIF technique relative to emission spectroscopy permits the use of much lower densities of excited OH, reducing the likelihood of metastable−metastable collisions that could give rise to competing processes that complicate the chemistry. The intense $A\ ^2\Sigma^+ - X\ ^2\Pi$ transition is suitable for detecting the populations of the lower v'' levels of the X state and has been used in a multitude of experimental and field studies, especially of the ground vibrational level. However, OH($A,v' \geq 2$) vibrational bands are strongly predissociated, with lifetimes in the 10−1000 ps range.[5,6] This limitation, in conjunction with the highly diagonal nature of the Franck−Condon factors for the $A-X$ system, restricts its application to OH($X,v'' \leq 4$ or 5).

In this paper, we discuss the alternative $B\ ^2\Sigma^+ - X\ ^2\Pi$ system with respect to OH(X,v'',J'') detection. Figure 1 shows potential energy curves for the OH X, A, and B states. The B state is quite shallow, with a bond dissociation energy D_e of about 1250 cm^{-1} and only two bound vibrational levels.[7] It has a much larger internuclear separation than that of the ground state, r_e = 1.8 Å, giving rise to intense $\Delta v \neq 0$ vibrational transitions. The $B-X$ $0-v''$ bands have significant Franck−Condon overlap
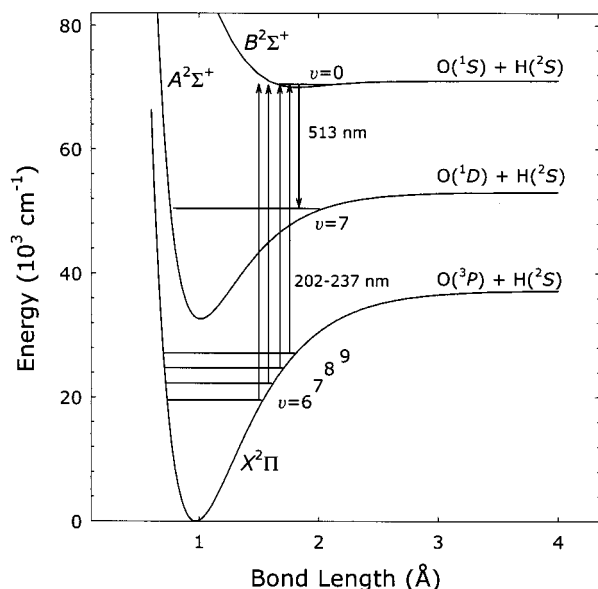

Figure 1. Potential energy curves for the OH X, A, and B states. The X and A potentials were approximated using a Morse function with parameters taken from Luque and Crosley;[23] the B-state potential was obtained from an ab initio calculation.[34] The $B-X$ 0–v'' bands excited in this work are shown, along with one of the $B-A$ bands detected in emission.

only for vibrational levels above about $v'' = 6$. The absorption intensity peaks for the 0–8 and 0–9 bands.[8] Copeland and co-workers first exploited this transition in OH LIF measurements in the late 1980s.[9,10] They have since used $B-X$ LIF data to better quantify spectroscopic term values for OH($X,v'' = 7–9,11–13$)[11,12] and also to measure a large number of collisional removal rate constants for OH($X,v'' = 7–12$).[13–16]

Because of the large $\Delta v \neq 0$ Franck–Condon factors, the $B-X$ transition is well suited for studying the nascent v'',J'' populations of reaction 1, which produces a highly inverted OH population peaking at $v'' = 9$, as well as the time evolution of the populations as dictated by quenching rate constants and decay pathways. In the present experiments, reaction 1 was used to populate OH($v'' = 6–9$), which was then detected using the $B-X$ 0–v'' bands as shown in Figure 1. The $B-X$ 0–5 transition occurs in the vacuum UV; its study would require additional experimental complexity and was not pursued. No attempts were made to detect populations in OH($X,v'' \geq 10$), which lie above the nominal 27 000 cm^{-1} exothermic limit of reaction 1. The fluorescence is easily detected by monitoring any one of a number of strong B $^2\Sigma^+ \rightarrow A$ $^2\Sigma^+$ transitions in the visible portion of the spectrum.[9]

This experiment was originally designed to permit reaction 1 to occur without collisional relaxation of the nascent OH(v'',J'') product populations. However, the spectral analysis that was performed after completion of data-taking showed that the nascent vibrational populations were partially relaxed by collisions and the rotational populations were equilibrated to approximately room temperature. The background pressure in the reaction chamber was very low ($10^{-4}-10^{-5}$ Torr), ensuring that collisional relaxation would be negligible during the residence time of a nascently formed OH(v'',J'') molecule. Instead, the observed relaxation probably resulted from the much higher density in the source region. This aspect of the experiment is discussed more fully below. Although the OH(v'',J'') nascent distribution from reaction 1 could not be determined, several aspects of the $B-X$ detection technique have been better characterized through this work. In particular, it is shown that
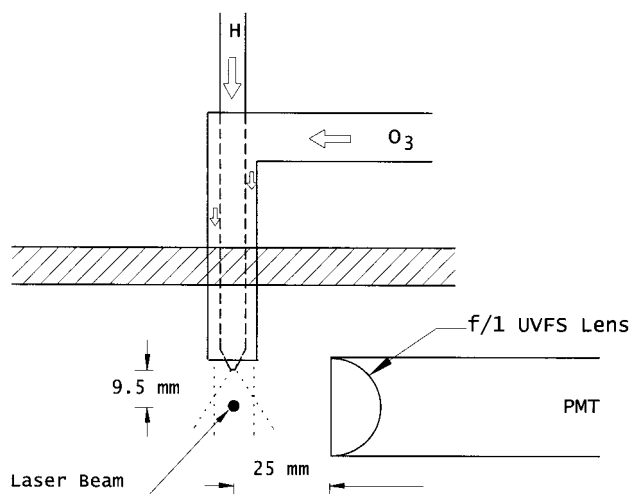
Figure 2. Close-up of the reaction region. Continuous flows of H atoms and ozone are introduced through concentric tubes into the vacuum region directly above a diffusion pump. The detection laser pulse intersects the gas expansion about 1 cm downstream of the H-atom nozzle. An *f*/1 UV fused silica lens collimates a portion of the fluorescence and directs it to a photomultiplier tube positioned on the outside of the reaction cell.

rotational state-dependent OH($X,v'' = 6–9$) populations can be obtained through synthetic spectral fitting of $B-X$ spectra, taking into account B-state predissociation effects. Populations in OH-($X,v'' = 6$) have been detected through the $B-X$ 0–6 transition for the first time. The $B-X$ 0–v'' relative emission intensities have been measured for comparison with existing theory. Finally, two separate simultaneously acting B-state predissociation mechanisms, induced by gyroscopic and spin–orbit coupling with the nearby 2 $^2\Pi$ state, have been identified by an examination of the observed J'-dependent lifetimes.

Experimental Section

The experiments were carried out in a 20 cm i.d. 6 cm high cell machined from aluminum and black-anodized to minimize reflections. The cell was bolted directly to the top of a Varian VHS-6 diffusion pump backed by a roughing pump. Fomblin 25/9 diffusion pump fluid (Kurt Lesker) was used to minimize decomposition by reaction with the ozone introduced into the chamber. The reagent gases were introduced through a port in the top flange. Ozone was prepared by flowing 99.5% O_2 through a commercial ozonator, then trapping the resultant ozone on a silica gel column cooled to -80 °C. The remaining O_2 was pumped off just prior to the experiment, and the O_3 was introduced through $^1/_2$ in. o.d. PFA Teflon tubing. Previous studies in our laboratory have indicated that nearly 100% pure O_3 can be supplied to the experiment in this manner.[17] Hydrogen atoms were produced by striking a microwave discharge in flowing H_2 gas, using a McCarroll cavity and a $^1/_2$ in. o.d. Pyrex tube that had been previously rinsed with orthophosphoric acid and distilled water, in turn, to minimize H-atom recombination on the glass surface. The H_2 was passed through a water bubbler prior to entering the microwave discharge in order the enhance the decomposition, which is typically about 30%. Total gas flows of 5.5–55 standard cm^3 min^{-1} were used, corresponding to background pressures from 3×10^{-5} to 3×10^{-4} Torr, with approximately equal flows of the O_3 and H-atom mixtures.

Figure 2 shows a detail of the gas inlet region. The H and O_3 were mixed using concentric tube inlets similar to those in the experiment of Charters et al.[1] The O_3 was passed through a $^1/_2$ in. o.d. Teflon pipe into the reaction chamber. The H-atom

mixture was passed through an interior $^1/_2$ in. o.d. Pyrex tube that had also been rinsed in orthophosphoric acid. The tube terminated in a nozzle with a $^1/_2$ or 1 mm opening. The detection laser beam probed the reaction mixture 9.5 mm downstream of the nozzle opening. A 25 mm diameter $f/1$ UV fused-silica lens was placed near the laser overlap region to increase the fluorescence collection efficiency. A Hamamatsu R928 photo-multiplier tube (PMT) was mounted on the exterior face of the reaction chamber to detect the resultant emissions, except for the $B-X$ $0-v''$ relative intensity study, where a Hamamatsu R166 solar-blind PMT was used. A Corning 3-72 long-pass filter (50% transmission at 455 nm) was used to eliminate laser scatter and isolate the strong OH $B-A$ emissions in the 475−550 nm region. Data were also obtained using a 512 nm center wavelength, 8 nm fwhm band-pass filter to isolate the strongest emission band, $B \rightarrow A$ $0-7$. However, it was later realized that this filter discriminated against high-J' emissions, biasing the population measurements. Data using this filter are not included in the present report.

The probe laser consisted of one of two dye laser-UV wavelength extender systems, with the dye lasers pumped by the frequency-tripled output of a 10 Hz Continuum 661S-10 Nd:YAG laser. For the 0−7, 0−8, and 0−9 bands at 213, 225, and 237 nm, respectively, a Lambda-Physik Scanmate 2E dye laser was used to generate tunable light in the 426−474 nm region using either C440 or C460 laser dye. The UV wave-lengths were obtained by frequency doubling the dye laser output in a BBO crystal mounted in an Inrad Autotracker III, allowing synchronous wavelength scanning. For the 0−6 band at 202 nm, a Continuum TDL-51 dye laser, running on a mixture of R610 and R640 dye, was used to generate 606 nm light. The output was frequency-doubled in a KDP crystal mounted in an autotracking Spectra-Physics WEX-1. The doubled light was split off from the residual fundamental beam, polarization-rotated 90° with a half-wave plate, and recombined with the fundamental. The two vertically polarized beams were then mixed in a BBO crystal mounted in the Autotracker III to generate 202 nm light. Both crystals were electronically angle-tuned during wavelength scans. For both doubling and tripling, the longer wavelengths were removed in an Inrad four-prism filter, which has compensation built in to prevent walkoff as the wavelength is scanned. Reflections of the dye laser output off UV fused silica windows were passed into a Burleigh 5500 pulsed wavemeter for absolute wavelength measurement, and through a 1.27 cm^{-1} free spectral range Etalon to provide a sinusoidal fringe pattern for wavelength linearization.[17] The latter was necessary to obtain accurate spectral fits, given the nonlinearities in the dye laser drive mechanisms. The probe laser fluence was relatively low (<30 μJ in a 3 mm diameter beam) to avoid saturation. This is a minor concern, because the $B-X$ transition is an order of magnitude weaker than the $A-X$ transition.

The data acquisition process, including dye laser monochro-mator scanning and fluorescence data acquisition and storage, was controlled using LabVIEW 5 running on a laboratory personal computer. The PMT output was amplified 25 times by an EG&G Ortec 535 fast current preamplifier and then passed to a LeCroy LC374A oscilloscope for digitization. The fluores-cence decay curves were typically integrated over 8−64 laser shots using a 150 ns gate width and then passed to the computer over an IEEE-488 interface. The UV probe laser fluence and Etalon trace were also recorded during wavelength scans. The raw spectra were divided by the fluence signal to account for long-term drift. The dye laser monochromator drives were
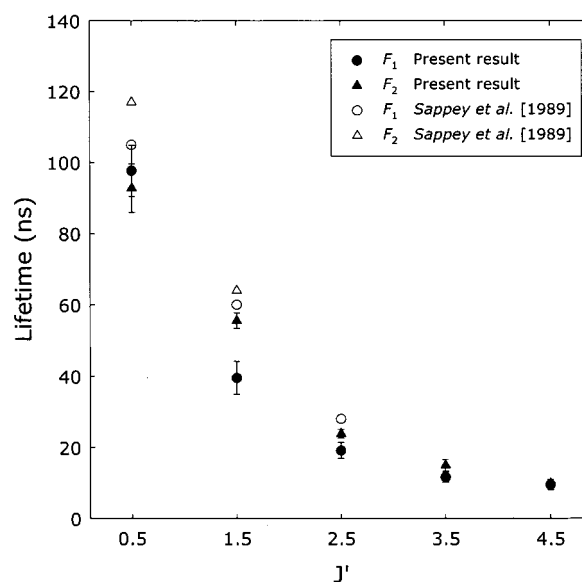
Figure 3. OH($B,v' = 0$) collision-free lifetimes, measured as a function of J'. The error bars shown correspond to 1-σ standard deviations in the mean of the measurements. Also shown are the values obtained by Sappey et al.[18] in a similar experiment. The estimated error bars for the Sappey et al. data are ±15% and ±50% for F_1 and F_2, respectively.

controlled over RS-232 interfaces using either in-house (TDL-51) or vendor-supplied (Scanmate 2E) instructions. Further numerical analysis was carried out on a DEC AlphaStation 250.

Results

B $^2\Sigma^+$ **State Collision-Free Lifetimes.** B $^2\Sigma^+$ state lifetimes were measured using the oscilloscope to calculate the time for the signal to decay from 90 to 10% of its maximum intensity, thus, avoiding potential nonexponential behavior at early and late times. The 90−10 decay time was converted to an e-fold time by dividing by a factor of 2.2. The possible effects of collisional quenching were checked by measuring the decay constant at two or three different background pressures; no dependence on pressure was observed. Figure 3 shows the lifetimes τ_{obs} measured for the lower J' levels of the B $^2\Sigma^+,v'$ $= 0$ vibrational state. The values for the F_1 levels are derived from pumping the $B-X$ $0-8$ P_1 rotational branch, and the values for the F_2 levels from the R_2 branch, avoiding excitation of the undesired B-state spin−rotation sublevel via a near-resonant $\Delta J \neq \Delta N$ satellite line. As can be seen, the lifetimes decrease rapidly with increasing J', reaching the limit of the current measurement capability at about $J' = 4.5$. The results are seen to be in good agreement with the values obtained by Sappey et al.[18] The relatively short lifetimes and their rapid decrease with J' are indicative of a weak predissociation process,[19] which is described in more detail below.

In an earlier report, Bergeman et al.[20] bombarded low-pressure water vapor with a pulsed 20 keV electron beam and then detected the time-dependent $B-A$ visible emission to deduce the lifetime of the B state. Their measured B-state lifetimes, in the 2−3 μs range, are more than a factor of 10 longer than the more direct present measurements and those of Sappey et al.[18] Given the unselective nature of the excitation source, the Bergeman et al. measurements may have been corrupted by radiative and/or collisional cascade from a higher-lying meta-stable electronic state. However, the same technique was used to determine A-state lifetimes which have proven quite accurate.[5] It should also be noted that neither Bergeman et al.[20] nor Felenbok,[21] in earlier work, recognized the importance of the

high-J' predissociation effect and incorrectly ascribed falloffs in rotational line intensity to anomalously low effective Boltzmann rotational temperatures. Sappey et al.[9] have shown that much higher effective temperatures are obtained when the predissociation is taken into account.

OH $B-X$ Spectral Data and Fits. Spectral data were obtained for the four $B-X$ $0-v''$ bands with $v'' = 6-9$. The data were then fit using a nonlinear least-squares algorithm described in detail previously.[17] Transition frequencies were calculated from literature rotational term values for OH(X,v'' $= 6-9$) and OH($B,v' = 0$).[12,22] In the absence of more accurate information, such as that which exists for the $A-X$ transition,[23] the rotational line intensities were taken to be equal to analytic Hönl−London factors.[24] Individual F_1 ($N = J - \frac{1}{2}$) and F_2 ($N = J + \frac{1}{2}$) J''-state populations were determined, with the fit constrained by the redundant information provided by the 12 allowed rotational branches. For each scan, two different fits were performed. In the first fit, the upper state collision-free lifetimes were constrained to the lifetimes measured in the direct time-domain measurements discussed above. In the second fit, the upper state lifetimes were allowed to vary. In that case, the fit determined the J' lifetimes relative to $J' = \frac{1}{2}$ from P, Q, and R branches probing the same lower state J'' population. The J'-dependent lifetimes determined from the spectral fits agreed with those measured in the time domain, with somewhat larger error bars. Because the time domain measurements are more precise, the OH populations were determined by fixing the lifetimes to values derived from those shown in Figure 3. Representative spectral data and associated synthetic spectral fits are shown in Figure 4 for $v'' = 8$ and 6, respectively.

Figure 5 shows representative populations for $v'' = 9$ and 8 determined from spectral fits. It is seen that the rotational and spin−orbit populations follow a Boltzmann dependence, with the effective temperature typically in the 300 K range. Previous studies[25,26] have shown that the nascent rotational population distribution arising from reaction 1 is highly excited, with effective temperatures near or above 1000 K for $v'' = 6-9$. Two vibrational levels were probed on each day of experiments in an attempt to confirm previously measured vibrational distributions. The vibrational populations were found to decrease as v'' increased from 6 to 9. Again, this is in contrast to the highly inverted distribution reported in the literature, which peaks at $v'' = 9$. Despite the low background pressure in the mid-10^{-5} Torr regime, it appears that collisions have significantly relaxed the nascently produced populations. This is somewhat surprising, given that Charters et al.,[1] with a similar source and higher background pressure, obtained much more inverted rotational and vibrational distributions.

As one test of the source conditions, a trace amount of NO, seeded in Ar, was passed through the nozzle injector in place of the H atom flow. Pure Ar was passed through the outer tube to replicate the flow and background conditions occurring in the H + O_3 reaction. An LIF spectrum was obtained using the NO A $^2\Sigma^+-X$ $^2\Pi$ $0-0$ band at 227 nm and then subjected to a nonlinear least-squares fit using well-established laboratory computer codes to determine the rotational temperature. This experiment was repeated by seeding the NO into the outer tube. The best-fit rotational temperatures were found to be 187 ± 9 and 274 ± 3 K for the inner and outer tubes, respectively, indicating that a significant amount of adiabatic expansion cooling is taking place out of the nozzle injector. It is conceivable, though probably unlikely, that this cooling has resulted in a population distribution that appears to be partially relaxed.
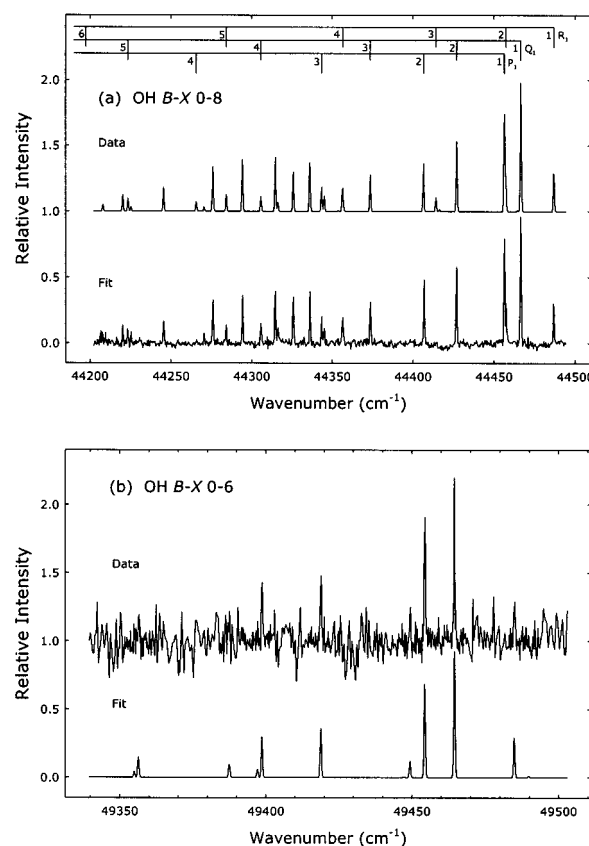
Figure 4. OH($B-X$) spectral data and synthetic spectral fits. The data have been normalized by the probe laser fluence. (a) $0-8$ vibrational band. Rotational line assignments for the three F_1-F_1 branches are shown at the top of the figure. There are twelve branches altogether, including the F_1-F_1 and F_2-F_2 main branches and the F_1-F_2 and F_2-F_1 satellite branches. (b) $0-6$ vibrational band.

More likely is that the nascently produced OH(v'',J'') have undergone some degree of collisional relaxation prior to detection. The OH($v'' = 6-9,J''$) populations are relaxed with rate constants in the 10^{-10} and $10^{-12}-10^{-11}$ cm^3 s^{-1} range for the rotational and vibrational degrees of freedom, respectively.[27,13] The observation of complete rotational relaxation and partial vibrational relaxation suggests that, on average, a nascent OH(v'',J'') molecule has undergone on the order of 10 collisions prior to detection. The source environment can be modeled assuming the H-atom mixture expands as a free jet into a low-density O_3 background gas that does not significantly impede the flow.[28] The gas density ρ decreases roughly as $\rho_o(X/d)^{-2}$, where X is the distance downstream of the nozzle and d is the nozzle diameter. The density ρ_o immediately downstream of the nozzle is equal to approximately one-half the stagnation density, or about 6×10^{16} cm^{-3}. The binary hard sphere collision frequency and the H + O_3 reaction rate decrease more rapidly than the gas density, however, owing to the temperature falling with X. The collision frequency has decreased by a factor of 10 at a downstream distance $X = d$, whereas the H + O_3 reaction rate has decreased an additional amount owing to the 470 K activation barrier. (The reaction is slowed by a factor of 2.5 at 187 K relative to room temperature,[29] with the room-temperature rate constant equal to 2.9×10^{-11} cm^3 s^{-1}.) Thus, the great majority of the OH(v'',J'') populations are formed immediately downstream of the nozzle. The 187 K gas temperature implies that the nozzle effluent has attained a Mach number of about 1.3, giving an initial velocity of 1250 m s^{-1}. At this velocity, the first millimeter downstream of the nozzle
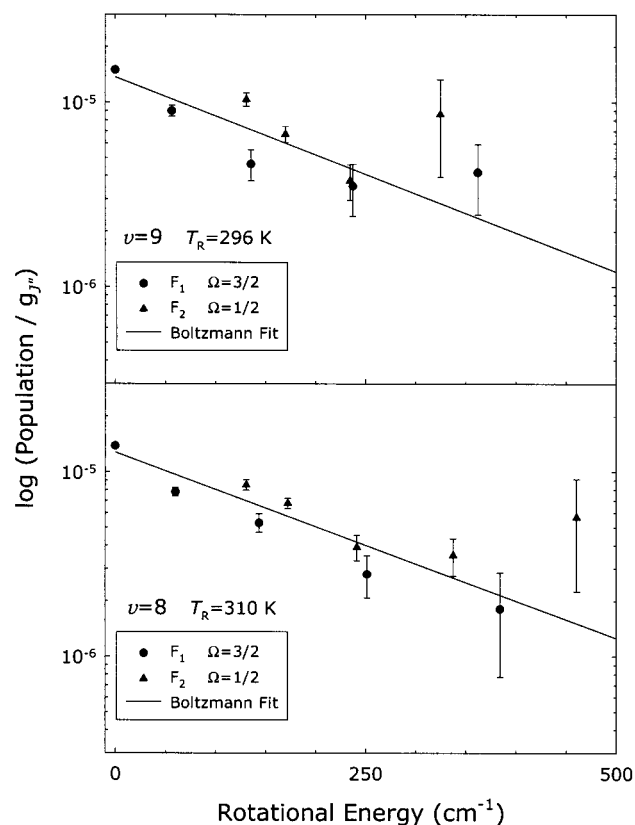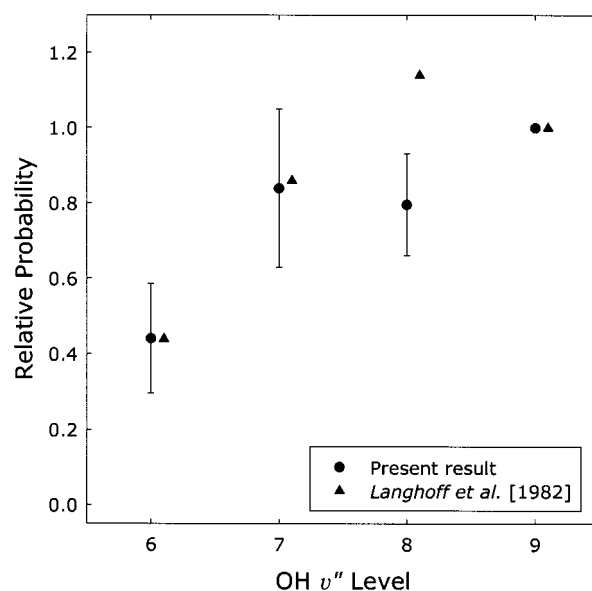
Figure 5. Best-fit OH(X,v'',J'') populations resulting from fits to $B-X$ LIF spectral data, for $v'' = 9$ (top) and $v'' = 8$ (bottom). In general, the populations were well fit to a Boltzmann distribution, with both the spin−orbit and rotational degrees of freedom equilibrated at approximately room temperature.

Figure 6. Einstein A coefficients for $0-v''$ bands in the OH($B-X$) system, normalized to A_{09}. The error bars shown correspond to 1-σ standard deviation in the mean of the best-fit values. Relative A-coefficient values calculated by Langhoff et al.[8] are shown for comparison. The experimental and theoretical results are offset slightly for clarity.

is covered in 1 μs, during which time about five collisions have occurred at an average pressure of 1 Torr. Although this represents only a simplistic model of the system, it is at least semiquantitatively consistent with the observed relaxation.

OH $B-X$ 0−v'' Vibrational Band Intensities. To better quantify the derived vibrational distribution, the $B-X$ 0−v'' band intensities for $v'' = 6-9$ were measured relative to that of the 0−9 band. This was accomplished by performing repeated wavelength scans over the strong $Q_1(J'' = {}^3\!/_2)$ transition for one of the four bands (e.g., 0−7), while monitoring the emission intensity at a wavelength corresponding to a different band (e.g., 0−8). The lifetime of the pumped upper state rotational level is limited by a combination of predissociation and emission via the much stronger $B-A$ band system. However, this lifetime is constant among the measurements because the same upper state vibration−rotation level is being populated. The $B-X$ system is relatively weak, with little or no signal observable using a monochromator to disperse the fluorescence. Thus, the $B-X$ 0−v'' emission bands were isolated using a set of 10 nm fwhm optical filters. The resulting line profiles were normalized to the pump laser fluence and fit to a Gaussian function to determine relative peak areas.

The PMT-filter relative response at each of the four wavelengths was measured using the pulsed UV laser output as the light source. The laser was reflected off a UV fused silica window and passed through a series of neutral density filters, lowering the fluence to less than 1 nJ to avoid saturating the PMT. The measurements were performed until the resultant slopes were consistent from day to day. The PMT response as a function of laser fluence was found to be linear over an order of magnitude in fluence. Account was taken of the calculated

20% larger window reflection efficiency at 202 nm relative to 237 nm. The neutral density filter transmission has been determined by the vendor (Optics for Research) to be wavelength independent in this region.

A total of 11 independent measurements were made comparing the emission intensities of pairs of $B-X$ 0−v'' bands. These 11 intensity ratios were then least-squares fit-to-three ratios that uniquely define the intensities relative to the 0−9 band. The results are shown in Figure 6. The error bars are relatively large owing to the weak intensities and corresponding small signal levels. The intensities are compared to the theoretical values determined by Langhoff et al.,[8] which have estimated error bars of ±20%. There is good agreement for the relative intensities of $B-X$ 0−6 and 0−7 Einstein A-coefficients relative to that for 0−9, with borderline agreement for 0−8. We consider the present results to provide good confirmation of the accuracy of the theoretical calculation.

Discussion

As mentioned in the Introduction, Copeland and co-workers have used the OH($B-X$) transition to great advantage in measuring rate constants for collisional removal of highly vibrationally excited OH($X,v'' = 7-12$).[13] In those studies, an OH(X,v'',J'') level was populated by exciting a lower-energy level via a vibrational overtone. A J'' level near or at the maximum in the Boltzmann distribution was pumped, to minimize rotational redistribution on the time scale of the vibrational relaxation. Using this strategy, only one J'' level was detected and OH(B) J'-dependent lifetime information was not necessary in the analysis. Also, because the Boltzmann population peaks at a low J'' value, the B-state predissociation did not seriously degrade the OH(X,v'',J'') detection sensitivity.

In this paper, we show that spectral, and thus J''-dependent, population information can be obtained from OH($B-X$) LIF spectra provided the upper state lifetimes are taken into account. The method is obviously limited to low J'' values by the predissociation. However, measurable low-J'' populations can

be extended to higher J'' values assuming a particular distribution, such as the Boltzmann distributions shown in Figure 5. It should be noted that the present measurements were made at very low background pressure and still exhibit superior S/N even with limited signal averaging. At higher pressures, or with an increased production rate, higher J'' levels may easily be detected. In some cases, absorption methods such as cavity ringdown spectroscopy (CRDS) may be better suited for experiments employing the $B-X$ band for detection, given the upper state predissociation limitation.[30] In our experiment, it was expected that the CRDS technique would have insufficient S/N for detecting the OH populations.

Figure 6 confirms the $B-X$ $0-v''$ vibrational band strengths calculated by Langhoff et al.[8] This agreement provides more confidence that accurate vibrational level populations can be derived from OH($B-X$) $0-v''$ data. Acceptable fits to the $0-v''$ spectral data were obtained assuming Hönl–London factors for the rotational linestrength dependence, constrained by the J'-dependent predissociation lifetimes. For $v' = 0-4$, $\Delta v = -3$ to $+4$ bands in the $A-X$ system, Luque and Crosley[23] found that increasing rotation improves the wave function overlap for bands with $\Delta v \neq 0$ (although the comparison is made more difficult because the $A-X$ system is diagonal). The improved wave function overlap is countered by the effects of the electric dipole transition moment function, which decreases with r for the internuclear separations sampled by most of the bands. For the internuclear separations sampled by the $B-X$ $0-v'' = 6-9$ transitions, with r-centroids in the $1.57-1.74$ Å range,[21] the r-dependent $B-X$ transition moment function has a negative slope similar to that for the $A-X$ system.[31] Rough comparison with the Luque and Crosley data suggests that these effects could modify the relative $B-X$ Hönl–London linestrengths over the $N'' = 1-5$ range by up to 30%, resulting in changes in the derived temperature of up to 15%. In principle, $B-X$ transition probabilities could be calculated in a manner similar to the Luque and Crosley analysis of the $A-X$ transition, because similar r-dependent transition dipole moment information is available, as well as a B-state potential curve to enable a calculation of the vibration–rotation wave functions via numerical integration.[8,31]

In addition to collisional removal of high-v'' OH, the $B-X$ detection technique can also be used to characterize the nascent distribution and decay pathways of OH(X,v'',J') populations resulting from reaction 1. The excited OH gives rise to the intense visible–near-IR Meinel band emissions in the mesopause region near 87 km altitude. The reaction also plays a controlling role in the amount of heating near the mesopause.[32] Both of these phenomena are influenced by the nature of the OH(v'',J'') product distribution and its quenching rates. Although this distribution has been measured in a number of published studies, major uncertainties remain.[2] Notably, all existing laboratory measurements were performed at ambient temperature, even though the reaction occurs in the atmosphere at temperatures in the $150-220$ K range. In general, the nascent product distribution could depend on temperature. Also, evidence in the work that examined the pressure dependence of the inferred product distribution[1,26] suggests that partial relaxation of the OH(v'',J'') product was occurring even at the lowest pressures used. Given the superior signal-to-noise inherent in LIF measurements, the $B-X$ detection technique could be used to extend the previous work to lower pressures. For the present setup, the source conditions would have to be adjusted to obviate the observed effects of collisional quenching. Assuming that
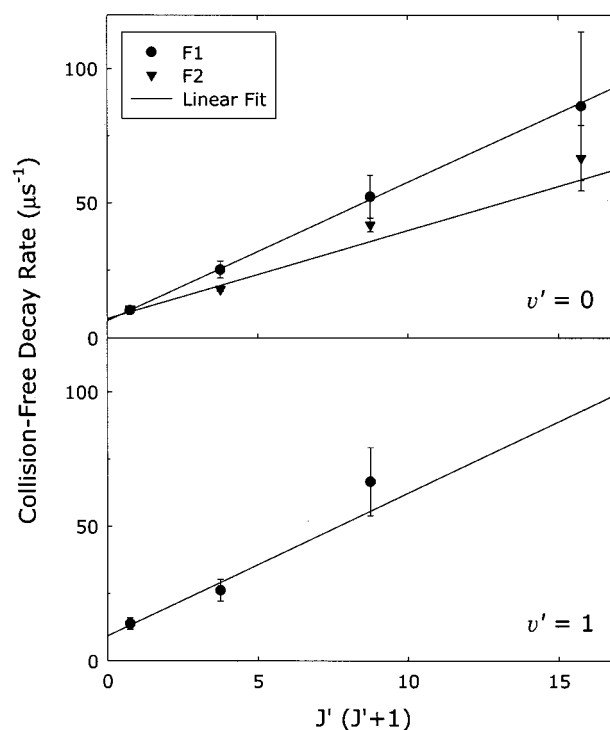

Figure 7. J'-dependent, collision-free decay rates for OH(B) $v' = 0$ (top) and $v' = 1$ (bottom). The values were determined from the lifetime data shown in Figure 3. For $v' = 0$, data from the present study were used; for $v' = 1$, data from Sappey et al.[18] were used.

could be done, it would be possible to employ a cooled injector to investigate the temperature dependence.

Predissociation Mechanism. Figure 7 shows the collision-free predissociation rates as a function of $J'(J' + 1)$. The values were derived by inverting the lifetimes shown in Figure 3. No correction was made for the nonresonant laser scatter decay time, measured to be $\tau_{\text{laser}} = 9.5 \pm 0.3$ ns. We estimate that deconvolving the laser scatter may add as much as several tens of percent to the highest J'-value predissociation rates, with smaller corrections for lower values of J'. This leads to increasing error in the decay times with J'. For the fastest decays, a large amount of signal averaging was performed to maximize the measurement precision. The currently measured inverse lifetimes for the F_1 and F_2 spin components of OH($B,v' = 0$) were used, along with the $v' = 1$ F_1 inverse lifetime values from Sappey et al.[18] The Sappey et al. data for $v' = 1$ F_2 spin components are imprecise owing to concurrent excitation of F_1 populations.

The observed J' dependence in the predissociation rate is characteristic of the effects of the **L**-uncoupling operator, one of the terms in the rotational portion, $\mathbf{H}^{\text{ROT}}$, of the molecular Hamiltonian that is neglected in the Born–Oppenheimer approximation. This interaction is often referred as a "gyroscopic" perturbation. Although the linear dependence on $J'(J' + 1)$ of the observed effect is also consistent with tunneling through a centrifugal barrier, the barrier tunneling mechanism is ruled out in the present case because the rotational levels involved lie well below the energy of the B-state dissociation limit. Felenbok[21] and Carlone and Dalby[7] report data identifying $v' = 0$, $N = 15$ and $v' = 1$, $N = 9$ as the highest bound rotational levels. These data, together with thermochemical data from other electronic states, suggest that $D_e(B\ ^2\Sigma^+)$ is approximately equal to 1250 cm^{-1}, with an estimated 100 cm^{-1} dispersion barrier near 3.8 Å internuclear separation. The **L**-uncoupling operator is a one-electron operator, and in the single configuration limit,

6036 *J. Phys. Chem. A, Vol. 105, No. 25, 2001*

Hwang et al.
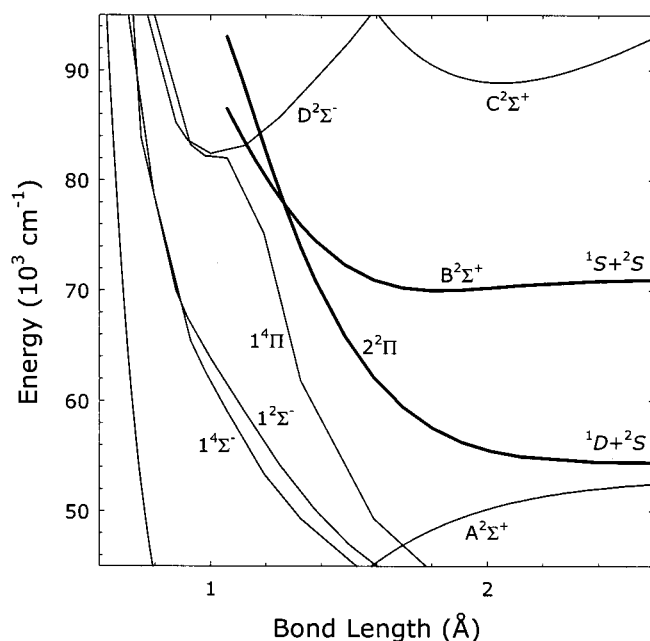
Figure 8. Potential energy curves for selected Σ and Π electronic states near the OH $B\ ^2\Sigma^+$ state. The $2\ ^2\Pi$ state, which crosses the $B\ ^2\Sigma^+$ state near the energy minimum, is responsible for spin–orbit and gyroscopic perturbation-induced predissociation; the two curves are shown in bold. The A- and C-state potential curves were approximated using Morse functions, whereas the remaining potentials were obtained from the ab initio calculations of van Dishoeck and Dalgarno[31] ($1\ ^4\Sigma^-$, $1\ ^2\Sigma^-$, $1\ ^4\Pi$, and $D\ ^2\Sigma^-$) and Schwenke[34] ($2\ ^2\Pi$ and $B\ ^2\Sigma^+$). All of the curves are referenced to T_e of OH(X).

the interacting state can differ from $B\ ^2\Sigma^+$ by at most one spin–orbital. Because the selection rules for a gyroscopic perturbation are $\Delta\Omega = \pm 1$, $\Delta\Lambda = \pm 1$, $\Delta S = 0$, and $\Delta\Sigma = 0$, the perturbing state must be a $^2\Pi$ state. As shown in Figure 8, the most obvious candidate is the repulsive $2\ ^2\Pi$ state, which intersects the $B\ ^2\Sigma^+$ potential near the minimum on the inner limb of the curve. The curves cross at about 1.27 Å, where the leading configurations of the $B\ ^2\Sigma^+$ and $2\ ^2\Pi$ states are $\sigma^2\pi^2(^1\Sigma^+)\sigma^*$ and $\sigma\pi^3(^1\Pi,^3\Pi)\sigma^*$, respectively; these differ by the requisite one spin–orbital.[31]

The gyroscopic coupling vanishes in the limit $J' \rightarrow 0$. Thus, in the absence of other predissociation mechanisms, the y intercept of Figure 7 should be inversely related to the radiative lifetime. However, the derived $J' = 0$ lifetime values for $v' = 0$ and $v' = 1$, 157 ± 4 and 139 ± 57 ns, respectively, are much shorter than the theoretical values of Langhoff et al.,[8] which were calculated neglecting nonradiative decay. For $v' = 0$ and $v' = 1$, Langhoff et al. calculated 300 and 515 ns, respectively, with $\pm 20\%$ error bars accounting for the range spanned by the lifetimes when the calculation was performed using three different kinds of basis sets. Assuming the calculation is accurate, the remaining nonradiative (i.e., predissociation) rate for $J' = 0$, in the $3-6\ \mu s^{-1}$ range, must be caused by a homogeneous perturbation, which is one whose strength does not depend on J'. Among the homogeneous perturbations, the spin–orbit coupling operator $\mathbf{H}^{SO}$ typically produces the strongest coupling when a nearby state exists obeying the appropriate selection rules. Like the $\mathbf{L}$-uncoupling operator, the spin–orbit coupling operator, $\mathbf{H}^{SO}$, can be well approximated as a one-electron operator, and the interacting state can differ by at most one spin–orbital. One of the most general selection rules for a spin–orbit-induced perturbation is $\Delta\Omega = 0$, which is satisfied by several of the states for which potential curves are shown in Figure 8. The states which, in principle, could

interact via $\mathbf{H}^{SO}$ with the $B\ ^2\Sigma^+$ state include those of $^2\Sigma^-$, $^2\Pi$, $^4\Sigma^-$, and $^4\Pi$ symmetry. However, inspection shows that the same $2\ ^2\Pi$ state is the leading candidate for the spin–orbit-induced homogeneous predissociation, again because of its proximity to the B-state potential well. For a state differing by one spin orbital, the selection rules for the spin–orbit interaction are $\Delta\Omega = 0$, $\Delta\Lambda = -\Delta\Sigma = \pm 1$, and $\Delta S = 0$ or ± 1. Of the $2\ ^2\Pi_{1/2}$ and $2\ ^2\Pi_{3/2}$ spin–orbit sublevels, only $2\ ^2\Pi_{1/2}$ can interact with $B\ ^2\Sigma_{1/2}^+$ owing to the $\Delta\Omega = 0$ requirement for a homogeneous perturbation.

To better quantify the predissociation, more precise measurements of the $J' = 0$ intercept and J'-dependent predissociation rates are required, as a function of the F_1 and F_2 sublevels and also of v'. From the theory point of view, this system is attractive because it appears to be dominated by a single perturbing state, $2\ ^2\Pi$. This is in contrast to the predissociation of the lower $A\ ^2\Sigma^+$ state, which arises from interactions with all three of the repulsive curves that intersect it, through various perturbation mechanisms.[6] Thus, the $B\ ^2\Sigma^+\sim 2\ ^2\Pi$ system may prove a useful test case for improved theoretical understanding of $^2\Sigma^+\sim^2\Pi$ predissociation effects in OH. Further calculations also offer the possibility of prediction of v',J',F_i-dependent predissociation rates, which would be of considerable value in converting observed emission rates from v',J' levels to accurate $v',J',F_i \leftarrow X\ (v'',J'')$ excitation rates. We will discuss this system in detail in a forthcoming publication.[33]

Summary

The reaction of H with O_3 has been used to produce OH in highly excited vibrational levels. The populations in these levels were probed via the $B\ ^2\Sigma^+ - X\ ^2\Pi\ 0 - v''$ bands. Spectral fitting has been used to determine OH(X,v'',J'') populations that have been partially relaxed by collisions. Relative intensities for the OH($B-X$) $0-v''$ bands with $v'' = 6-9$ have been measured and agree well with a published ab initio calculation. Several collision-free OH($B,v' = 0$) rotational state lifetimes have also been determined. They decrease rapidly with J', in agreement with a previous measurement. The $B\ ^2\Sigma^+$ state is predissociated by a combination of spin–orbit and gyroscopic interactions with the nearby repulsive $2\ ^2\Pi$ state. Although the upper state predissociation limits the LIF detection technique to the study of levels with relatively low J'' values, LIF via the $B\ ^2\Sigma^+$ state exhibits much higher S/N than OH chemiluminescence detection. This may facilitate more detailed studies of the collisional decay pathways, at lower OH metastable densities to minimize competing chemistry.

References and Notes

(1) Charters, P. E.; Macdonald, R. G.; Polanyi, J. C. *Appl. Opt.* **1971**, *10*, 1747.

(2) Klenerman, D.; Smith, I. W. M. *J. Chem. Soc., Faraday Trans. 2* **1987**, *83*, 229 and references therein.

(3) Dupuis, M.; Fitzgerald, G.; Hammond, B.; Lester, W. A.; Schaefer, H. F., III. *J. Chem. Phys.* **1986**, *84*, 2691.

(4) Yu, H. G.; Varandas, A. J. C. *J. Chem. Soc., Faraday Trans.* **1997**, *93*, 2651.

(5) Brzozowski, J.; Erman, P.; Lyyra, M. *Phys. Scr.* **1978**, *17*, 507.

(6) Parlant, G.; Yarkony, D. R. *J. Chem. Phys.* **1999**, *110*, 363.

(7) Carlone, C.; Dalby, F. W. *Can. J. Phys.* **1969**, *47*, 1945.

(8) Langhoff, S. R.; van Dishoeck, E. F.; Wetmore, R.; Dalgarno, A. *J. Chem. Phys.* **1982**, *77*, 1379.

(9) Sappey, A. D.; Crosley, D. R.; Copeland, R. A. *J. Chem. Phys.* **1989**, *90*, 3484.

(10) Sappey, A. D.; Crosley, D. R.; Copeland, R. A. *J. Chem. Phys.* **1990**, *92*, 818.

(11) Copeland, R. A.; Chalamala, B. R.; Coxon, J. A. *J. Mol. Spectrosc.* **1993**, *161*, 243.

(12) Coxon, J. A.; Sappey, A. D.; Copeland, R. A. *J. Mol. Spectrosc.* **1991**, *145*, 41.

(13) Dyer, M. J.; Knutsen, K.; Copeland, R. A. *J. Chem. Phys.* **1997**, *107*, 7809 and references therein.

(14) Knutsen, K.; Dyer, M. J.; Copeland, R. A. *J. Chem. Phys.* **1996**, *104*, 5798.

(15) Chalamala, B. R.; Copeland, R. A. *J. Chem. Phys.* **1993**, *99*, 5807.

(16) Sappey, A. D.; Copeland, R. A. *J. Chem. Phys.* **1990**, *93*, 5741.

(17) Dodd, J. A.; Lockwood, R. B.; Hwang, E. S.; Miller, S. M.; Lipson, S. J. *J. Phys. Chem. A* **1999**, *103*, 7834.

(18) Sappey, A. D.; Crosley, D. R.; Copeland, R. A. *Adv. Laser Sci. IV, Conf. Proc.* **1989**, *191*, 645.

(19) Lefebvre-Brion, H.; Field, R. W. *Perturbations in the Spectra of Diatomic Molecules*; Academic Press: Boston, MA, 1986.

(20) Bergeman, T.; Erman, P.; Larsson, M. *Chem. Phys.* **1980**, *54*, 55.

(21) Felenbok, P. *Ann. Astrophys.* **1963**, *26*, 393.

(22) Coxon, J. A.; Foster, S. C. *Can. J. Phys.* **1982**, *60*, 41.

(23) Luque, J.; Crosley, D. R. *J. Chem. Phys.* **1998**, *109*, 439.

(24) Earls, L. T. *Phys. Rev.* **1935**, *48*, 423.

(25) Llewellyn, E. J.; Long, B. H. *Can. J. Phys.* **1978**, *56*, 581.

(26) Polanyi, J. C.; Sloan, J. J. *Proc. Symp. Chem. Kinet. Data*; Benson, S. W., Ed.; Wiley: Ney York, 1975; p 51.

(27) Kliner, D. A. V.; Farrow, R. L. *J. Chem. Phys.* **1999**, *110*, 412.

(28) Miller, D. R. In *Atomic and Molecular Beam Methods*; Scoles, G., Ed.; Oxford University Press: New York, 1988; Vol. 1, Chapter 2.

(29) DeMore, W. B.; Sander, S. P.; Howard, C. J.; Ravishankara, A. R.; Golden, D. M.; Kolb, C. E.; Hampson, R. F.; Kurylo, M. J.; Molina, M. J. *JPL Publ.* **1994**, 94−26.

(30) Spaanjaars, J. J. L.; ter Meulen, J. J.; Meijer, G. *J. Chem. Phys.* **1997**, *107*, 2242.

(31) van Dishoeck, E. F.; Dalgarno, A. *J. Chem. Phys.* **1983**, *79*, 873.

(32) Mlynczak, M. G.; Solomon, S. *J. Geophys. Res.* **1993**, *98*, 10517.

(33) Field, R. W.; Clevenger, J. O.; Schwenke, D. W.; Dodd, J. A. **2001**, manuscript in preparation.

(34) Schwenke, D. W. **2001**, personal communication.